ACS Catalysis

Research Article

pubs.acs.org/acscatalysis

Speciation of Ruthenium as a Reduction Promoter of Silica-Supported Co Catalysts: A Time-Resolved in Situ XAS Investigation

Jingping Hong,[†,‡,§,¶] Eric Marceau,*[,†,‡] Andrei Y. Khodakov,*[,§] Lucia Gaberová,[†,‡] Anne Griboval-Constant,[§] Jean-Sébastien Girardon,[§] Camille La Fontaine,[∥] and Valérie Briois*[,∥]

[†]Sorbonne Universités, UPMC Univ Paris 06, UMR 7197 CNRS, Laboratoire de Réactivité de Surface, F-75005 Paris, France

[‡]CNRS, UMR 7197 CNRS, Laboratoire de Réactivité de Surface, F-75005 Paris, France

[§]Unité de Catalyse et de Chimie du Solide, UMR 8181 CNRS, Bât. C3, Université Lille 1, 59655 Villeneuve d'Ascq, France

[∥]Synchrotron SOLEIL, L'Orme des Merisiers, BP48, Saint-Aubin, 91192 Gif-sur Yvette, France

Supporting Information

ABSTRACT: Complete reduction of the metal phase in cobalt-containing catalysts is often difficult to reach and can be promoted by a small amount of noble metals. Because these costly promoters are introduced in a very low quantity, their speciation and their chemical interaction with cobalt have seldom been studied in detail. We present here a time-resolved in situ X-ray absorption spectroscopy investigation of the speciation of ruthenium, used as a reduction promoter of cobalt, throughout the preparation of Co/SiO_2 catalysts. In the cobalt(II) nitrate impregnation solution, ruthenium is detected as hydrated $Ru(OH)_4$ short-chain oligomers that are deposited on silica upon drying. Co_3O_4 forms during calcination in air and catalyzes the elimination in the gas phase of 60% of Ru. The addition of a polyol, sorbitol, in the impregnation solution stabilizes the whole of Ru on the catalyst. Upon calcination, Ru(IV) ions are inserted inside Co_3O_4 nanoparticles. Reduction of the oxidic phase takes place in two distinct steps, at approximately the same temperatures regardless of the ruthenium content: first to Ru(III)-containing CoO nanoparticles (Ru ions modifying the intrinsic electronic properties of the oxidic nanoparticles); then to bimetallic Co nanoparticles containing Ru(0) atoms, via an autocatalytic process. Ru loadings as low as 0.2 wt % are sufficient to afford complete reduction of cobalt. Close association between Ru and Co from the beginning of the synthesis is thus necessary for a maximum promoting effect.

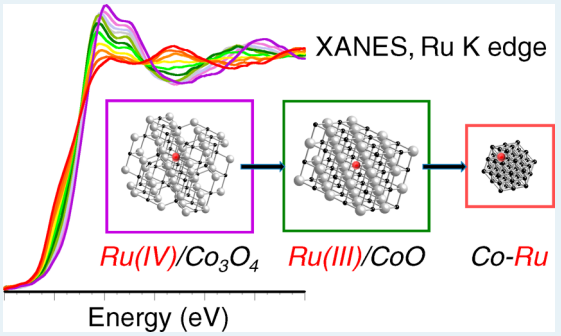

KEYWORDS: *ruthenium, cobalt, reduction promoter, in situ study, X-ray absorption spectroscopy, Fischer−Tropsch synthesis*

INTRODUCTION

Bimetallic nanoparticles exhibit specific properties in catalysis that often derive from the synergy between the two metals. Much work has been focused on nanoparticles based on a combination of noble metals because of their chemical stability and their easy reduction to the metallic state. Combinations of two base metals, or of one base metal with one noble metal, also lead to systems with enhanced catalytic activities or selectivities, and to a benefit in terms of cost. The noble metal can play specific roles toward the base metal, such as promoting its reduction.[1−4] Because the type of association between the two metals (alloy, core−shell structure, segregation) influences the properties and reactivity of the nanoparticles, it is important to follow the fate of the promoter throughout the synthesis, in order to optimize its mode of introduction and, when possible, to optimize its loading. This is a challenging task because noble metals may be used in very small quantities and thus will not respond to X-ray diffraction or other conventional structural techniques. Moreover, the structure and morphology of the nanoparticles may evolve upon changing gas atmosphere. To get insight into the speciation of reduction promoters in realistic conditions, selective and highly sensitive in situ characterization techniques must be implemented.

A key catalytic reaction which can benefit from the use of noble metals as reduction promoters is the Fischer−Tropsch synthesis (FTS). This process allows transforming syngas, a mixture of CO and H_2 produced from natural gas, coal, or biomass, into clean hydrocarbons that are convenient substitutes for diesel fuels produced by oil refining.[5−14] Industrial FTS applications have been based on iron or cobalt, the latter being more active, more selective in medium-chain alkanes, and less prone to deactivation. Cobalt nanoparticles are supported on oxides such as silica, alumina, or titania, but because of the chemical interactions between cobalt oxide and support, complete cobalt reduction into catalytically active metal nanoparticles can be difficult.

For this reason, small amounts of Pt, Re, Ir, or Ru are added to the catalyst formulation to increase the fraction of reduced

Received: November 12, 2014
Revised: January 15, 2015
Published: January 15, 2015

DOI: 10.1021/cs501799p
ACS Catal. 2015, 5, 1273−1282

cobalt and, as a consequence, the catalytic activity.[1,3,15−19] But where the promoter is located in the catalyst is not always clear. In the case of Ru, former research has led to contradicting conclusions. Ru is sometimes assumed to be located inside[1,20−22] or at the surface of[22−24] bimetallic Co−Ru nanoparticles, although other studies postulate the existence of individual monometallic Ru nanoparticles segregated on the support,[2,21,25−27] raising the question of their role not only in cobalt reduction but also in catalysis. Another specificity of Ru is its volatility in oxidative conditions, which may result in a loss of the reduction promoter before it has fulfilled its function.[3,27,28] Understanding the chemistry of Ru during the synthesis of the catalysts is thus crucial if one wants to optimize their preparation and the catalyst properties.

X-ray absorption spectroscopy, whether under in situ conditions or not, has been applied to the characterization of supported FTS catalysts.[13,15,29−38] Jacobs, Davis et al. have successfully developed in situ Quick X-ray absorption spectroscopy (Quick-XAS) at the Co K edge as a way to assess the aptitude of metal promoters to favor the reduction of cobalt oxide to metallic nanoparticles.[15,18,37] A report on the stepwise reduction of promoters Pt and Ag has also been published recently.[19] In the present paper, we will show that Quick-XAS applied to Co−Ru/SiO_2 catalysts at the Ru K edge under in situ conditions provides invaluable information on the fate of the ruthenium promoter from the impregnated to the final, reduced system. To the best of our knowledge, this is the first time that the speciation of the promoter is followed throughout the preparation of supported nanoparticles, both in controlled atmosphere and in time-resolved conditions. We will aim at explaining the chemical process of Ru volatilization, the enhanced reducibility of Co−Ru/SiO_2 compared to Co/SiO_2 systems, and the way chemical interactions are established between Ru and Co. Lastly, by using sorbitol as an organic additive in the impregnation solution,[31] we will also show that it is possible to stabilize ruthenium while improving the dispersion and spatial distribution of metallic nanoparticles over the silica support.

EXPERIMENTAL SECTION

Catalyst Preparation. Commercial silica (CARiACT Q-10, 75−150 μm, S_{BET} = 300 m^2/g, total pore volume = 1.33 cm^3/g, pore diameter = 7.3 nm) was used as support. Co−Ru/SiO_2 catalysts were prepared by incipient wetness impregnation of silica with an aqueous solution containing both cobalt(II) nitrate hexahydrate and ruthenium(III) nitrosyl nitrate, without or with addition of sorbitol $HOCH_2(CHOH)_4CH_2OH$. All chemicals were supplied by Aldrich. Co and Ru contents were fixed at 10 and 0.5 wt % respectively, corresponding to a Ru/Co atomic ratio of 1/40. Catalysts are labeled as "CoRu/SiO_2" and "CoRu-sorb/SiO_2" depending on the presence of sorbitol in the impregnation solution. When applicable, the sorbitol/Co molar ratio is 1/10. Impregnated samples were dried in air at room temperature overnight and activated in an O_2/He flow (20% of O_2 in He, 38 cm^3 min^{-1}) up to 400 °C with a heating ramp of 2 °C min^{-1} from room temperature to 250 °C, and 5 °C min^{-1} from 250 °C to 400 °C. After purging and cooling to room temperature under He, catalysts were reduced in a diluted H_2 flow (5% H_2 in He, 32 cm^3 min^{-1}) up to 500 °C with a heating ramp of 7 °C min^{-1}. Ru/SiO_2 and Ru-sorb/SiO_2 samples, prepared without cobalt and exhibiting RuO_2 and Ru(0) nanoparticles after oxidative activation and reduction, respectively, were also synthesized as references. In all thermal treatments, He was used as a dilutant instead of N_2 or Ar, in order to minimize absorption of the X-rays by the gas atmosphere.

Characterization. Ru K edge and Co K edge Quick X-ray absorption spectra (XANES and EXAFS) were obtained in situ in the transmission mode, during oxidative activation and reduction of the catalysts, on SAMBA beamline at synchrotron SOLEIL (Gif-sur-Yvette, France). The beamline is equipped with two Quick-XAS monochromators. The Si (311) channel-cut crystal was used for the Ru K edge measurements, whereas the Si(111) channel-cut crystal was used at the Co K edge.[39] The oscillation frequency was 1 Hz, taking 500 ms to obtain one spectrum. A mass of 0.150 or 0.035 g of catalyst was sampled for recording at the Ru and at the Co edges, respectively. The catalyst was loaded as a powder into the XAS reactive cell designed at SOLEIL,[40,41] where it was maintained between two metallic frits and exposed to a flow of gas while heated, using the experimental parameters listed in the former section. The volume between the frits was partly filled in with small pieces of graphite sheets for experiments at the Co K edge involving less catalyst powder. The energy was calibrated to the first inflection point of a cobalt metal foil, or of a rhodium foil in the case of Ru. At the Ru K edge, EXAFS signals were averaged over 400 spectra, in order to optimize the signal-to-noise ratio (the edge jump being less than 0.1).

XAS analysis was performed using the Athena software.[42] After pre-edge and atomic background removal, XANES spectra were normalized in the middle of the first EXAFS oscillation. Multivariate-Curve Resolution by Alternative-Least Squares (MCR-ALS) methodology, first proposed by Tauler in 1995,[43] was used for the quantification of chemical phases during reduction. The MCR-ALS method applied to X-ray absorption spectroscopy was detailed in recent papers.[44−46] The principle of the procedure is presented as Supporting Information (SI, pp. S1−S2). The als2004 graphical interface developed by the Tauler's group[47] is freely available as a Matlab toolbox. The sets of spectra recorded at the Co and Ru edges could be explained using three components.

χ(k) EXAFS spectra were Fourier-transformed (without phase correction) using a k^3-weighting and a Kaiser-Bessel window (in the k range of 4.4−13.5 $Å^{-1}$ at the Ru K edge, and 3.0−11.5 $Å^{-1}$ at the Co K edge, with dk = 1 in both cases). The procedures for the analysis of spectra at the Co K edge have been presented elsewhere.[30] At the Ru K edge, the ATOMS and FeFF6 packages were employed to generate ab initio phase and amplitude functions for the Ru−O, Ru−Ru, and Ru−Co atom pairs, using the Artemis interface.[48] RuO_2 and reduced Ru-sorb/SiO_2 sample (Ru(0) nanoparticles) were used for testing the transferability of these pair functions for the treatment of the catalyts. Structural parameters R (average interatomic distance from the emitting atom), N (coordination number), and σ (Debye−Waller factor) were determined by multiple k-weight least-squares fitting procedures, to better distribute the sensitivity of the evaluation of the goodness-of fit parameter χ^2 over the entire k range. The corresponding overall r-factor reported for each sample derives from the nonlinear least-squares minimization of χ^2 for all k-weights (k^1, k^2, k^3); it differs from the r-factors per data set also reported for each k-weight in the output file. χ^2 and r-factor metrics are defined by the IXS standards and criteria committee (http://ixs.iit.edu/subcommittee_reports/sc/err-rep.pdf). For the sake of clarity in results presentation, peak positions on Fourier transforms will be referred to by the values read on axis x of the figures,

DOI: 10.1021/cs501799p
ACS Catal. 2015, 5, 1273−1282

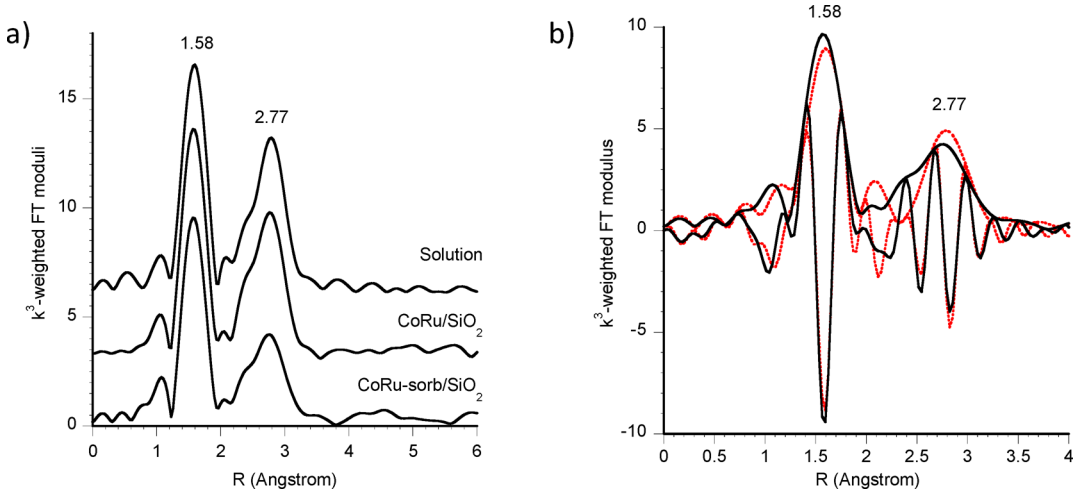

Figure 1. (a) Ru K EXAFS k^3-weighted Fourier transform moduli of the ruthenium precursor solution and dried samples $CoRu/SiO_2$ and $CoRu\text{-}sorb/SiO_2$; (b) Results of k^3 $\chi(k)$ EXAFS fitting in R-space of dried $CoRu\text{-}sorb/SiO_2$ (black: experimental; red: fit).

which differ by a few tenths of angstroms from the real interatomic distance *R*, obtained from EXAFS fitting and listed in the tables.

Diffuse reflectance infrared Fourier transform (DRIFT) spectra were recorded with a resolution of 4 cm^{-1} (128 scans averaging) on a Bruker IFS66 V spectrometer equipped with an MCT (mercury cadmium telluride) detector and a high-temperature environmental chamber (Spectratech), during an oxidative treatment similar to the activation performed on the catalysts.

X-ray diffraction (XRD) patterns were recorded at room temperature on a Siemens D5000 diffractometer using Cu Kα radiation (λ = 0.15418 nm). Scans were recorded in the 2θ range between 20 and 70° using a step of 0.02° and a step time of 5 s. The average size of Co_3O_4 particles was evaluated according to the Scherrer equation using the (311) peak located at 2θ = 36.9°.

H_2-temperature-programmed reduction (TPR) profiles were obtained by flowing a 5% H_2/Ar gas mixture through the catalysts while increasing the temperature at a linear rate, using a Micromeritics Autochem system. The sample loading in the quartz reactor was 0.1 mg. The gas flow velocity was 30 cm^3 min^{-1} with a temperature ramping rate of 7 °C min^{-1}, similar to the operating conditions of the reduction step in XAS measurements.

Bright-field and high angle annular dark field (HAADF) images were collected on a high-resolution transmission electron microscope (HRTEM) Jeol JEM-2010 at an accelerating voltage of 200 keV. Nanoparticle size was evaluated after sampling of more than 500 nanoparticles.

The number of surface metal sites in the catalysts was evaluated by propene chemisorption in a pulse reactor.[49] After reduction in pure hydrogen at 400 °C for 5 h, the catalyst sample (0.2 g) was cooled to 50 °C and purged with He for several hours. Pulses of propene (0.25 mL) were introduced into a flow of He. The number of metal surface sites was estimated from the amount of chemisorbed propene. It should be noted that because no assumption was made about the stoichiometry of propene chemisorption, this method provides only relative information about the concentration of cobalt metal sites in a series of similar catalysts.

Catalytic Measurements. Activity measurements were carried out in a fixed-bed stainless-steel tubular reactor (d_{int} = 8 mm) operating at atmospheric pressure with a H_2/CO molar ratio of 2. The catalyst loading was typically 0.5 g. Before reaction, the samples were reduced in situ in hydrogen flow at 400 °C for 5 h. CO contained 5% nitrogen, which was used as an internal standard. Analysis of H_2, CO, CO_2, and CH_4 was performed with a 13X molecular-sieve column, whereas hydrocarbons (C_2–C_{20}) were separated in 10% CP-Sil5 on a Chromosorb WHP packed column. The selectivity of hydrocarbons was calculated on carbon basis. The two catalysts described in the present paper are compared to catalysts prepared without Ru and described in ref 31.

RESULTS AND DISCUSSION

Speciation of Ru upon Impregnation and Drying. Figure 1a shows the three Fourier transforms (FT) calculated from EXAFS signals (without phase correction) recorded at the Ru K edge on the impregnation solution and on dried $CoRu/SiO_2$ and $CoRu\text{-}sorb/SiO_2$.

An intense peak assigned to second-nearest neighbors is clearly visible at 2.77 Å, which indicates that the speciation of ruthenium has evolved in solution from its monomeric Ru(III) nitrosyl form. Fitting in the R-space for $CoRu\text{-}sorb/SiO_2$ (Figure 1b) suggests that Ru atoms are the main contributors to this peak (results of the fits and discussion, fit in the R-space for $CoRu/SiO_2$, fits in the k-space, experimental EXAFS signals: SI, pp S3–S5, Figure S1). Different condensed Ru species originating from the oxidation and hydrolysis of ruthenium ions in nitrate-containing aqueous solutions have been hypothesized in the literature[50−54] and were tested for modeling. The Ru–Ru distance is consistent with that found in $Ru(IV)(OH)_4$ oligomers (also called hydrated or hydrous "$RuO_2{\cdot}xH_2O$"), described as existing inside zeolite cages.[51] The moderate quality of the fit between 2 and 2.5 Å on the FT prevents us though from drawing more precise conclusions on the degree of oligomerization of Ru(IV), or on condensation with cobalt ions at this early stage.

Transformations and Speciation of Ru during Oxidative Activation. In our previous reports on XAS at the Co K edge, we have shown that upon oxidative activation, hydrated cobalt(II) nitrate first dehydrates into anhydrous $Co(NO_3)_2$, then decomposes into Co_3O_4 nanoparticles, in line with XRD and with the literature.[30,31]

DOI: 10.1021/cs501799p
ACS Catal. 2015, 5, 1273−1282

In the first stage of oxidative activation, XANES spectra recorded at the Ru K edge do not change significantly compared to the dried catalysts. However, above 130 °C, the intensity of the edge jump starts decreasing for $CoRu/SiO_2$, revealing the elimination of Ru as a volatile species. In contrast, no change of edge jump intensity is observed for CoRu-sorb/SiO_2 (experimental XANES spectra are presented in the SI, p S6, Figure S2). It must be noted that when Ru/SiO_2 and Ru-sorb/SiO_2 are thermally treated in oxidative atmosphere (i.e., in the absence of cobalt), the Ru content is not modified. The presence of sorbitol on Ru-sorb/SiO_2 only shifts the formation of RuO_2 to 240−270 °C, instead of 220−250 °C on Ru/SiO_2.

The evolution of the Ru weight content, calculated from the intensity of the Ru K edge jump, is reported in Figure 2 (white and black circles). On the same figure is recalled a quantitative analysis of cobalt nitrate conversion into Co_3O_4, extracted from XANES data at the Co K edge for $CoRu/SiO_2$ (white squares) and published formerly.[30]

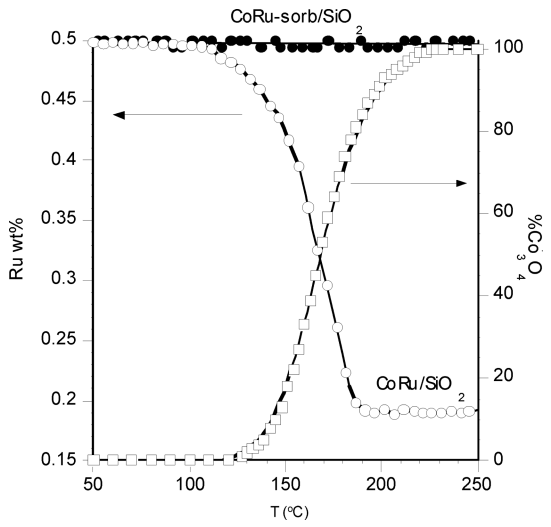

Figure 2. Left axis: evolution of the Ru weight content in $CoRu/SiO_2$ (white circles) and CoRu-sorb/SiO_2 (black circles) during oxidative activation, from in situ XANES measurements at Ru K edge. Right axis: evolution of the formation of Co_3O_4 in $CoRu/SiO_2$ (white squares), from in situ XANES measurements at Co K edge.

These results suggest a correlation between the elimination of Ru in the gas phase and the decomposition of cobalt nitrate into Co_3O_4, in the temperature range 130−190 °C. According to thermodynamics, the transformation of RuO_2 or monometallic Ru into volatile RuO_4 in an oxidative atmosphere is not favored below 800 °C.[55−57] However, it is known from electrochemistry studies that unlike bulk RuO_2, hydrated "$RuO_2{\cdot}xH_2O$", which is one of the compounds proposed to be present after drying and which has been reported to be stable above 100 °C, can readily be oxidized into RuO_4 when contacted with oxidizing catalysts, such as Ag(II) or Ce(IV).[58−60] Gaseous RuO_4 itself exhibits a half-life of 5 h at 90 °C[61] and could be metastable in these operating conditions.

Starting with hydrated molecular forms of Ru(IV), the elimination of ruthenium as RuO_4 could thus be rationalized, with two assumptions: Ru and Co are close enough after the drying step; Co(III) ions from freshly formed Co_3O_4 catalyze the reaction between Ru(IV) and oxygen, present in the gas atmosphere or released upon cobalt nitrate decomposition. The elimination of Ru would stop at 190 °C either because ruthenium has become entrapped inside oxidic nanoparticles and is not accessible any more at the solid−gas interface, or because water coordinated to Ru has been eliminated and dehydrated phases cannot be oxidized into RuO_4.[59] The elimination of Ru would not occur on CoRu-sorb/SiO_2 because, in the presence of sorbitol, the cobalt precursor decomposes into Co_3O_4 only above 210 °C;[31] that is, at a temperature for which the transformation of hydrated "$RuO_2{\cdot}xH_2O$" into RuO_4 is not favored any more. The loss of Ru in the gas phase would thus be linked to the initial speciation of Ru in solution.

Given the low quantity of sorbitol on the catalyst, it was not possible to determine precisely under which form sorbitol was present during the middle part of oxidative activation. A weak absorption band, absent from spectra recorded for $CoRu/SiO_2$, was detected by DRIFT at 1660 cm^{-1}, in the region of carbonyls, between 140 and 240 °C. The organic species stabilizing metal ions (cobalt, possibly ruthenium given the 20 °C shift in temperature observed for the formation of RuO_2 on Ru-sorb/SiO_2 compared with Ru/SiO_2) might thus be oxidized

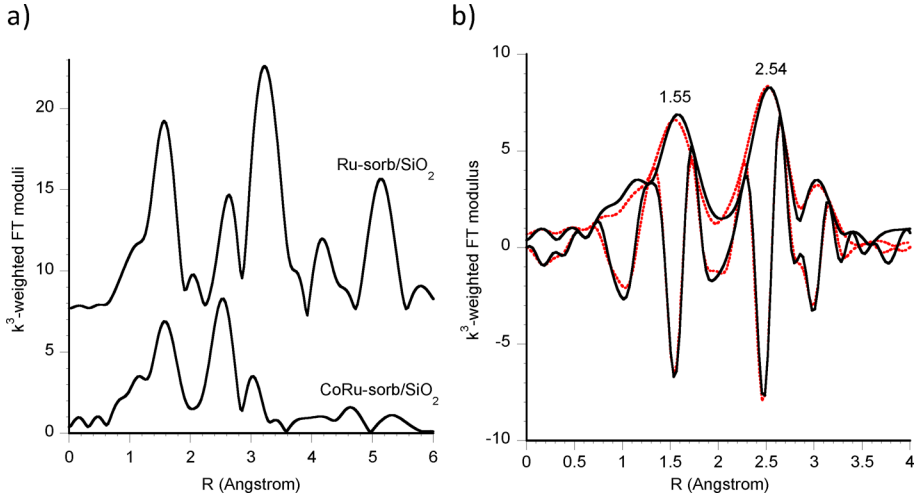

Figure 3. (a) Ru K EXAFS k^3-weighted Fourier transform moduli of samples Ru-sorb/SiO_2 (RuO_2) and CoRu-sorb/SiO_2 after oxidative activation; (b) Results of k^3 $\chi(k)$ EXAFS fitting in R-space of CoRu-sorb/SiO_2 after oxidative activation (black: experimental; red: fit).

DOI: 10.1021/cs501799p
ACS Catal. 2015, 5, 1273−1282

derivatives with coordinating properties, as has been assumed formerly (gluconic acid, or saccharic acid when sucrose is the additive[3,31]).

After completion of the oxidative treatment, EXAFS signals recorded at the Ru K edge are identical on both catalysts. The Fourier transform obtained for calcined CoRu-sorb/SiO_2 is shown in Figure 3, along with that of RuO_2 nanoparticles formed during oxidizing activation of Ru-sorb/SiO_2. The rutile structure of RuO_2 is characterized by two peaks of next-nearest neighbors above 2.5 Å on the FT (Ru−Ru distances: R = 3.107 and 3.535 Å[52]), the second one being the more intense. In contrast, a major peak, more intense than the peak of first neighbors, is observed at a shorter distance for CoRu-sorb/SiO_2. We have tested the hypothesis of the insertion of Ru(IV) ions into another crystalline oxidic phase, Co_3O_4. This hypothesis was first advanced by Iglesia et al.[1] and was based on the fact that calcination in oxidizing conditions promotes the interaction between the two metals; however, it has seldom been taken up in the literature.[25,29,62]

The size of Ru(IV) ions (0.62 Å)[63] is compatible with that of Co(III) ions (0.61 Å),[64] whereas Ru(III) ions are slightly larger (0.68 Å).[64] Indeed, substituting a Ru(IV) ion to a Co(III) ion in an octahedral cationic site results in a satisfactory fit of the EXAFS data, in particular with a good coincidence between the modeled and experimental imaginary parts for the three peaks (Figure 3b, Table 1; SI, pp. S7−8, Figure S3). Results of the fit are in agreement with the coordination numbers deduced from the spinel structure (6 O atoms and two different shells of 6 Co atoms). Next-nearest neighbors are found at 2.95 and 3.46 Å (octahedral and tetrahedral cobalt, respectively), compared with 2.87 and 3.35 Å in the pure Co_3O_4 spinel structure.[65] The substitution of Ru(IV) in a tetrahedral site occupied by Co(II) is much less convincing, with the major peak of next-nearest neighbors clearly shifted to larger distances (SI, p S7, Figure S3). The validity of this interpretation has been confirmed by an investigation at the Ru L_2 edge of Ru-sorb/SiO_2 and CoRu-sorb/SiO_2 on beamline LUCIA at synchrotron SOLEIL, and comparison with the literature[66−72] (SI, pp S9−10, Figure S4). The addition of Ru neighbors, as they would appear in individual particles or clusters of RuO_2, was tested but rather decreased the quality of the fit.

Table 1. Fitted Parameters at the Ru K Edge (E_0 = 22118 ± 3 eV, S_0^2 = 0.92) and Co K edge (E_0 = 7717.0 ± 0.5 eV, S_0^2 = 0.73)

backscatterer	N	σ^2 (Å^2) × 10^3	R (Å)
Ru K edge			
calcined CoRu-sorb/SiO_2			
O	6.2 ± 0.4	5.3 ± 0.7	2.02 ± 0.01
Co	5.9 ± 0.5	7.3 ± 0.6	2.95 ± 0.01
Co	5.9 ± 1.4	13.2 ± 2.2	3.46 ± 0.03
r-factor = 0.0022899, χ^2 = 109, N_{ind} = 12, N_{var} = 9			
reduced CoRu-sorb/SiO_2: intermediate species (MCR-ALS)			
O	6.4 ± 0.7	5.3 ± 1.2	2.09 ± 0.01
Co	11.3 ± 1.6	13.6 ± 1.5	3.09 ± 0.01
r-factor = 0.025466049, χ^2 = 132, N_{ind} = 11, N_{var} = 6			
reduced CoRu-sorb/SiO_2: final state			
Co	8.2 ± 1.3	6.2 ± 1.6	2.55 ± 0.01
Ru	2.6 ± 1.0	6.2 ± 1.6	2.60 ± 0.02
r-factor = 0.00106971, χ^2 = 60, N_{ind} = 7, N_{var} = 5			
Co K edge			
Co foil			
Co	12.0	6.3 ± 0.3	2.49 ± 0.01
r-factor = 0.000165738, χ^2 = 150, N_{ind} = 7, N_{var} = 4			
reduced CoRu/SiO_2			
Co	10.0 ± 0.6	15.6 ± 0.8	2.47 ± 0.01
r-factor = 0.000443332 χ^2 = 144, N_{ind} = 7, N_{var} = 4			
reduced CoRu-sorb/SiO_2			
O	1.8 ± 0.6	6.9 ± 4.3	1.96 ± 0.01
Co	5.4 ± 0.7	9.1 ± 1.1	2.48 ± 0.01
r-factor = 0.000488010, χ^2 = 39, N_{ind} = 7, N_{var} = 6			

r-factor: overall fit quality factor, χ^2: chi-square goodness-of-fit test, N_{ind}: maximum number of independent points in the data, N_{var}: number of variables in the fit.

In conclusion, on coimpregnated catalysts, the oxidative decomposition of the Co and Ru precursors leads to Ru(IV)-doped Co_3O_4 nanoparticles, whose structure cannot be distinguished by XRD or XAS at the Co K edge from that of pure Co_3O_4, due to the broadening of the diffraction peaks and to the low content in ruthenium (1 Ru atom for 40 Co). At low temperatures, cobalt(III) ions formed upon decomposition of cobalt(II) nitrate are supposed to catalyze the oxidation of hydrated $Ru(OH)_4$ into volatile RuO_4, resulting in a loss of Ru. Sorbitol, or one of its oxidized derivatives, may act as a coordinating agent and stabilize metal cations out of the temperature domain where RuO_4 forms.

Speciation of Ru during and after Reduction. Before reduction, Ru(IV)-doped Co_3O_4 nanoparticles exhibit a size evaluated by XRD as 11.2 and 7.0 nm for CoRu/SiO_2 and CoRu-sorb/SiO_2 respectively. These values are similar to those measured for their counterparts prepared without Ru[30] and confirm that sorbitol contributes to decreasing the average nanoparticle size.

Figure 4 shows the temperature-reduction profiles (TPR) of the two catalysts. In line with the literature[1,20,27,31,73,74] and regardless of the average particle size, reduction takes place in two distinct steps, with maxima around 190 °C and above 360 °C. A quantitative analysis by a MCR-ALS procedure of XANES-TPR data recorded at the Co K edge up to 500 °C provides evidence of the characteristic contributions of cobalt

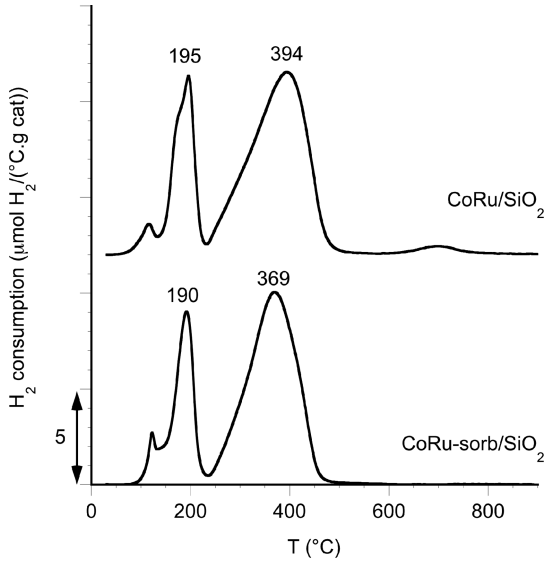

Figure 4. Temperature-programmed reduction profiles of CoRu/SiO_2 and CoRu-sorb/SiO_2.

DOI: 10.1021/cs501799p
ACS Catal. 2015, 5, 1273−1282

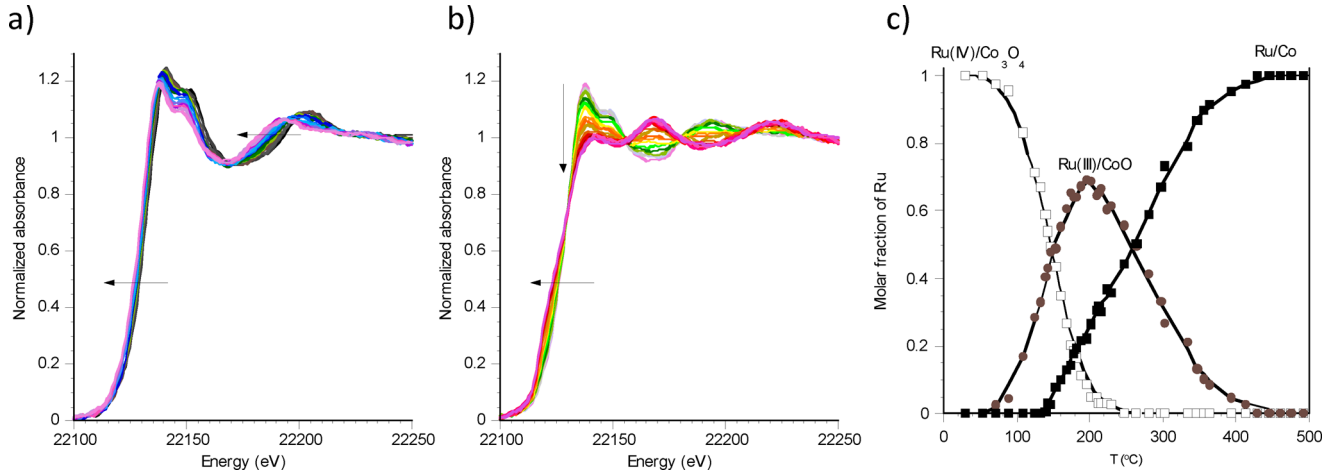

Figure 5. Reduction of ruthenium monitored on CoRu-sorb/SiO_2 by in situ Ru K XANES-TPR measurements: (a) between 29 and 200 °C (from black to purple); (b) between 200 and 500 °C (from gray to dark pink); c) speciation of the Ru phases as a function of temperature during reduction determined by MCR-ALS analysis.

oxides[31,75,76] and confirms the stepwise reduction of Co_3O_4 first to CoO, then to a reduced form of cobalt (SI, pp S11−14, Figures S5−S10). In the 20−500 °C range, TPR and XANES-TPR results are consistent, though some temperature shifts of the reduction peaks were evidenced when comparing the two techniques (SI, p. S13, Figure S8). They were attributed to differences in the geometry of the two reactors, in terms of diameter, height, and packing of the catalyst bed.

According to TPR (Figure 4), reduction is quasi-complete at 500 °C, and the small reduction peak at 700 °C (cobalt silicate) observed for CoRu/SiO_2 is minor compared with the intense high-temperature peaks observed in the absence of Ru (SI, p S13, Figure S7). Though Ru loading is 60% lower on CoRu/SiO_2 before reduction starts, there is no major negative consequence on cobalt reducibility.

The evolution of Ru speciation during reduction was investigated on CoRu-sorb/SiO_2. This sample was selected for the sake of sensitivity, because it contained more Ru than CoRu/SiO_2 after oxidative activation. XAS results obtained after oxidative activation and TPR profiles being similar, we will suppose that the evolution of Ru speciation follows the same route for the two catalysts.

The set of Ru K edge XANES spectra recorded as a function of temperature is presented in Figure 5 and can be divided into two series. Between 90 and 200 °C, the edge and first EXAFS oscillation shift to lower energies, denoting a decrease in Ru oxidation state and changes in its chemical environment. The XANES spectrum does not change much around 200 °C. Above 200 °C, the edge shifts again toward lower energies, and the white line progressively becomes extinct, leading to a spectrum similar to that of Ru(0).

Unlike the more complex processes taking place during oxidative activation of the catalyst, XANES-TPR data at the Ru K edge could be successfully interpreted on the basis of three components only, extracted by MCR-ALS analysis: the initial XAS spectrum of the oxidized catalyst (Ru(IV)-doped Co_3O_4), the one of the final, reduced catalyst, and a third one revealing the existence of an intermediate species (SI, p S15, Figure S11). EXAFS fitting of this MCR-ALS component leads to tendencies consistent with the chemistry of the system, with an intermediate phase consisting of Ru ions located inside the NaCl structure of CoO. The best fit suggests a first shell of 6.4 ± 0.7 O neighbors and a second shell of 11.3 ± 1.6 Co next-nearest neighbors (to be compared with the theoretical values, 6 and 12 respectively) and a good coincidence for the imaginary parts (Table 1; SI, p S15, Figure S11). An estimation of the concentration profiles for the three components is presented as a function of temperature in Figure 5c. Initially, the reduction of Ru parallels that of cobalt, from Ru(IV) inside Co_3O_4 nanoparticles to, presumably, Ru(III) inside CoO nanoparticles (Ru(II)-containing oxidic phases being extremely rare[77]). Metallic Ru is first detected around 150 °C, before Ru(III)/CoO has been completely formed. It can be noted that 150 °C is also the temperature at which RuO_2 nanoparticles are observed to reduce to Ru(0) on Ru-sorb/SiO_2. The full reduction of Ru to the metallic state takes place progressively, from 150 to 500 °C.

The enhancement by Ru of Co_3O_4 reducibility to CoO has sometimes been reported[1,21] and is also observed here (compare Figure 4 and Figure S7). Our results tend to contradict a hypothesis proposed in the literature, according to which Ru metallic nanoparticles, formed at the very beginning of the reduction process, activate hydrogen and trigger the reduction of Co_3O_4 to CoO.[78,79]

An alternative explanation based on the intrinsic properties of the doped Co_3O_4 nanoparticles may be found in the electrochemistry literature. Co_3O_4 is a semiconducting oxide, whose electric conductivity has been shown to increase both upon a temperature rise and upon doping with Ru(IV) ions.[80,81] Moreover, the upper layers of Ru-doped oxidic nanoparticles are reported to be slightly enriched in Ru.[61,64,82,83] Both phenomena could concur in increasing the reducibility of the oxide into Ru(III)/CoO, by facilitating the electron transfer from adsorbed hydrogen to the conduction band of the nanoparticles. We will comment below on the influence of Ru on the second reduction step, from CoO to metallic Co.

After completion of reduction, XAS spectra were recorded at room temperature, still under H_2 atmosphere, first at the Co K edge. It is recalled here that given the very low Ru/Co atomic ratio (1/40), Ru is unlikely to be detected by XAS in the vicinity of Co atoms. On CoRu/SiO_2, cobalt is present as metal, with Co−Co distances identical to those measured in the Co foil (Table 1; SI, pp S16−17, Figures S12−S13). The number

DOI: 10.1021/cs501799p
ACS Catal. 2015, 5, 1273−1282

of nearest Co neighbors is lower than 12 though, in line with the presence of nanoparticles in which the number of surface, under-coordinated atoms is not negligible. The EXAFS signal and FT of CoRu-sorb/SiO_2 require two contributions for a better fit: one from Co atoms in metallic cobalt, with a low coordination number, and one from O atoms. With respect to the fact that reduction of Co proceeds no further after an isothermal plateau at 500 °C (XANES), that it appears to be complete on the TPR profiles, and that the Co−O distance (1.96 Å) would be short for cobalt oxidic or silicate species, we will suppose that these O atoms are associated with a fraction of very small Co nanoparticles in interaction with the oxygen atoms of the silica surface. The existence of such small nanoparticles (≤2 nm) has been postulated on Co/γ-Al_2O_3 catalysts when Pt was the promoter.[27] It can be noted that the Debye−Waller factor for the Co shell on CoRu/SiO_2 and uncertainty on σ^2 for the O shell on CoRu-sorb/SiO_2 are quite large, implying a disorder or a variety in the supported cobalt species.

The state of ruthenium in reduced CoRu-sorb/SiO_2 can be deduced from the EXAFS data at the Ru K edge (Figure 6; fit in

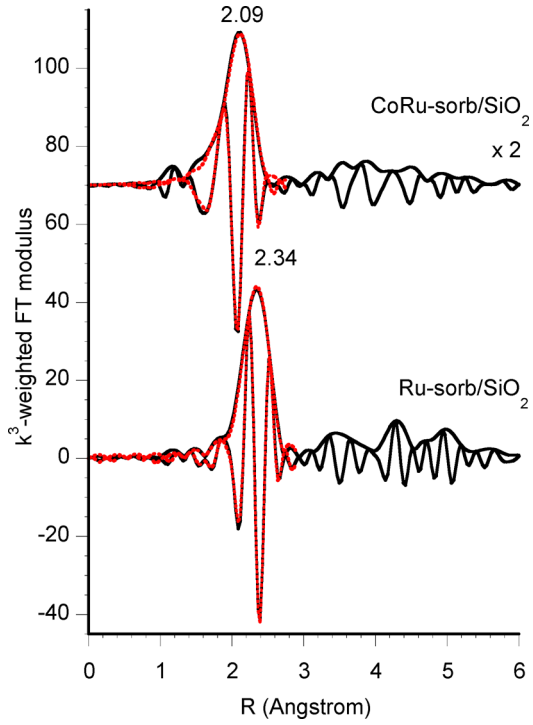

Figure 6. Ru K EXAFS k^3-weighted Fourier transform moduli (shifted vertically) and EXAFS fittings for the first shell of neighbors of the following: reduced Ru-sorb/SiO_2 and reduced CoRu-sorb/SiO_2 (black: experimental, red: fit).

k-space and experimental EXAFS signals: SI, pp S18−19, Figure S14; evolution of FT along the preparation of CoRu-sorb/SiO_2: SI, p S20, Figure S15). A comparison with metallic Ru (reduced Ru-sorb/SiO_2) clearly shows that the peak of nearest neighbors is located at a significantly shorter distance on CoRu-sorb/SiO_2. Fits obtained by surrounding Ru by Co atoms only were not favored because of large shifts of the energy parameter (3 eV below the error bar mentioned in the title of Table 1). Actually the best fit for the first shell, obtained by varying the total number of neighbors and the Ru/Co fraction of atoms involved as first neighbors (σ^2 being supposed identical for both elements) includes about 8 Co atoms and 2 Ru atoms, with a Ru−Co distance intermediate between the Co−Co and the Ru−Ru distances.[1,29] Independent fits for Ru and Co neighbors led to higher uncertainties on N and σ^2, but did not challenge the values of N and R. It can be noted that unlike Co K edge fitting, no oxygen neighbor was required to improve the fit.

It can thus be concluded that in majority, ruthenium introduced by coimpregnation forms truly bimetallic nanoparticles with cobalt, remaining embedded as individual atoms or small clusters after a two-step reduction process (Figure 7). This is in line with earlier interpretation by Iglesia et al.[1] and with experimental results obtained with rhenium and platinum as reduction promoters.[16,18,19] A recent report has rather concluded on the existence of bimetallic Co-containing Ru nanoparticles, on the basis of XAS recorded at the Ru K edge.[84] In that case, catalysts were prepared by sequential impregnation on a formerly calcined Co catalyst, which may explain the differences in terms of interactions between Co and Ru.

One can suppose that during the second step of reduction, Ru(III) is progressively reduced to Ru(0) atoms at the surface of CoO nanoparticles, enabling hydrogen activation for the further reduction of Ru(III)/CoO to the metallic state, in an autocatalytic process. A few teams have suggested that Ru could ultimately be stabilized under the surface of reduced Co nanoparticles, rather than at their surface,[20,73] and this may be supported by the absence of O neighbors around Ru and high number of metallic neighbors in the final reduced state. Moreover, as shown below, catalytic tests did not exhibit any significant differences in selectivity between nonpromoted and Ru-promoted Co catalysts, which suggests similar nature of active sites in both systems; it should be stressed though that sintering and reconstruction of the smaller cobalt nanoparticles under reaction cannot be ruled out.

Nevertheless, the presence of very small Ru nanoparticles formed above 150 °C and segregated over silica cannot be completely excluded, as it is in accordance the following: with the temperature of formation of Ru(0) from RuO_2; with the possible presence of Ru neighbors in the reduced state; and with the short Ru−Ru distance (usually reported as 2.66−2.68 Å[1,29]). Indeed, it is often proposed that the ease of reduction of cobalt in the presence of ruthenium can be due to hydrogen spillover from individual Ru nanoparticles toward cobalt species.[20,23,24,73,79,85] However, the addition of Ru neighbors, as they would appear in individual particles of RuO_2 or metallic Ru, to the fits of oxidized CoRu-sorb/SiO_2 and of the Ru-containing intermediate species isolated by MCR-ALS, respectively, has resulted in a decrease of the fit quality and in irrelevant values of N or R. If present on the support, small Ru nanoparticles seem to represent a minor fraction of ruthenium species.

The size and spatial distribution of the metallic nanoparticles on both catalysts were determined by transmission electron microscopy after their re-exposure to air (SI, p S21, Figure S16). In the absence of sorbitol in the preparation, particles appear as agglomerates in some zones of the silica support, whereas the distribution is more uniform due to the dispersing effect of sorbitol. On CoRu-sorb/SiO_2, the size of the nanoparticles is lower than 5 nm; this upper value is close to that obtained with sucrose as an organic additive.[3] In contrast, on CoRu/SiO_2, 25% of the nanoparticles are larger than 5 nm and measure up to 12 nm. The combination of Ru and sorbitol in the catalyst preparation thus ensures a high degree of

DOI: 10.1021/cs501799p
ACS Catal. 2015, 5, 1273−1282

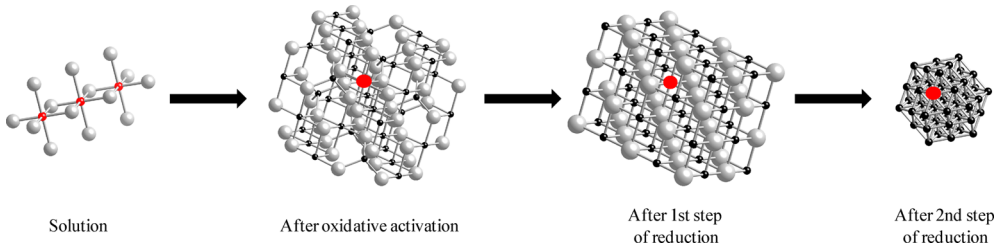

Figure 7. Speciation of Ru from the impregnation solution to the reduced state of catalyst CoRu-sorb/SiO_2 (atomic ratio Ru/Co = 1/40). Red: ruthenium; black: cobalt; gray: oxygen.

Table 2. Catalytic Performance in CO Hydrogenation of Cobalt-Based Catalysts Prepared with or without Ru and Sorbitol

catalyst	CO conversion (%)	selectivities (%)					cobalt-time yield (mol CO mol Co $^{-1}$ s^{-1}) × 10^4	adsorption of propene (μmol g_{catal}^{-1})
		CH_4	C_2	C_3	C_4	C_{5+}		
Co/SiO_2	4.7	8.7	4.6	4.6	6.2	75.9	2.0	22.3
Co-sorb/SiO_2	3.8	9.8	4.5	5.4	7.1	73.2	1.6	18.7
$CoRu/SiO_2$	8.8	9.1	3.0	3.9	4.9	79.1	3.7	32.8
CoRu-sorb/SiO_2	14.5	9.9	2.8	4.6	5.5	77.2	6.1	65.1

Reaction conditions: m_{catal} = 0.5 g, P = 1 bar, T = 190 °C, GHSV = 1800 mL g_{catal}^{-1} h^{-1}, H_2/CO = 2.

reduction of cobalt, higher cobalt dispersion and the formation of bimetallic Co−Ru nanoparticles without elimination of the noble metal as volatile oxide.

Catalytic Properties. Catalytic activities and products selectivities are listed in Table 2. The catalytic activity of each catalyst is seen to be about proportional to the concentration of cobalt surface sites evaluated by propene chemisorption. When sorbitol is added in the preparation of the catalyst in the absence of ruthenium (Co-sorb/SiO_2), the catalytic activity is lower than on reference Co/SiO_2 despite a smaller size of cobalt nanoparticles, due to a lower fraction of reduced metal. Methane selectivity slightly increases, also in line with the smaller size of nanoparticles. When ruthenium is present in the catalysts, a significant increase of the CO hydrogenation rate is observed, because cobalt is now completely reduced. The cobalt-time yield of $CoRu/SiO_2$ is almost twice larger than the one of Co/SiO_2 catalyst. The effect of ruthenium promotion is even more pronounced when sorbitol is used in conjunction with Ru. The reaction rate of CoRu-sorb/SiO_2 is about three times larger and four times larger compared with Co/SiO_2 and Co-sorb/SiO_2, respectively. The conversion measured for CoRu-sorb/SiO_2 is higher than for $CoRu/SiO_2$ because of these two fully reduced catalysts, the former contains the smaller nanoparticles, more evenly distributed on the support surface. Another consequence of the decrease of the nanoparticles' size is the slight increase of methane selectivity for CoRu-sorb/SiO_2, which parallels the observations made on the catalysts prepared without ruthenium.

CONCLUSION

Time-resolved Quick X-ray absorption spectroscopy experiments, performed under in situ conditions throughout the preparation of coimpregnated Co−Ru/SiO_2 systems, give access to the speciation and evolution of ruthenium, used at a low loading as a reduction promoter of supported cobalt nanoparticles.

In the impregnation solution and in dried catalysts, ruthenium is detected as hydrated $Ru(OH)_4$ short-chain oligomers. Upon formation of Co_3O_4 during calcination, ruthenium(IV) ions follow two diverging paths: elimination in the gas flow as RuO_4, resulting from the catalytic oxidation of $Ru(OH)_4$ by Co_3O_4; migration into the octahedral sites of the oxidic nanoparticles. Organic molecules added in the impregnation solution, such as sorbitol, act as stabilizers toward metal cations, retard cobalt nitrate decomposition up to temperatures at which RuO_4 does not form and favor the insertion of ruthenium ions inside Co_3O_4. Sorbitol is also found to enhance the dispersion and spatial distribution of metal nanoparticles all over the support surface.

Reduction of the mixed cobalt−ruthenium oxidic phase takes place in two steps, at approximately the same temperatures with any ruthenium content inside Co_3O_4, first to Ru(III)-containing CoO nanoparticles, then to bimetallic Co nanoparticles containing Ru(0) atoms. The enhancement of reducibility associated with Ru for the first reduction step may be assigned to changes in the semiconducting properties of Ru-doped Co_3O_4 nanoparticles. Though the presence of very small individual Ru metallic nanoparticles in a minor amount cannot be ruled out, XAS results tend to favor an autocatalytic mechanism for the second reduction step, in which Ru(III) ions at the surface of CoO nanoparticles are primarily reduced to metallic Ru. Ru(0) then activates hydrogen for the complete reduction of the two metals and formation of the bimetallic nanoparticles.

Comparison with the literature suggests that ruthenium speciation on catalysts is highly preparation-dependent. We show that its effectiveness as a promoter may even stem from the initial speciation of the metal in solution. Our study underlines the importance of associating ruthenium and cobalt for the maximum synergetic effect from the early stages of the bimetallic nanoparticles preparation, which is possible through coimpregnation of the oxidic support and use of organic additives. Cobalt reduction is promoted even at a low level of ruthenium doping. Introducing organic additives such as sorbitol in the impregnation solution is shown to be a cheap and convenient way to prevent ruthenium loss in the gas phase, which would be particularly crucial if a very low loading of reduction promoter were used.

DOI: 10.1021/cs501799p
ACS Catal. 2015, 5, 1273−1282

■ ASSOCIATED CONTENT

Supporting Information

The following file is available free of charge on the ACS Publications website at DOI: 10.1021/cs501799p.

Fits of XAS data in the k- and in the R-spaces; experimental spectra and EXAFS signals recorded at the Ru K edge; XAS study at the Ru L_2 edge; in situ XAS at the Co K edge; principle of the MCR-ALS procedure and MCR-ALS components; TPR and XANES-TPR data; bright field and HAADF-HRTEM micrographs (PDF)

■ AUTHOR INFORMATION

Corresponding Authors

*E-mail: eric.marceau@upmc.fr.

*E-mail: andrei.khodakov@univ-lille1.fr.

*E-mail: valerie.briois@synchrotron-soleil.fr.

Present Address

[¶]Key Laboratory of Catalysis and Materials Science of the State Ethnic Affairs Commission and Ministry of Education, South-Central University for Nationalities, Wuhan, China.

Notes

The authors declare no competing financial interest.

■ ACKNOWLEDGMENTS

The French National Agency for Research is thanked for financial support of this work (ANR-07-BLAN-0265; grant: X-ray absorption spectroscopy for operando catalyst characterization). SOLEIL is acknowledged for the use of synchrotron radiation on beamlines SAMBA (project no. 20100272) and LUCIA. The authors thank Patricia Beaunier and Jean-Marc Krafft (Laboratoire de Réactivité de Surface, UPMC) for their help in carrying out HAADF-HRTEM and DRIFTS measurements, respectively. V.B. also thanks Ludovic Duponchel (LASIR, Lille) for his advice in the use of the als2004 routine used for the MCR-ALS XAS data resolution.

■ REFERENCES

(1) Iglesia, E.; Soled, S. L.; Fiato, R. A.; Via, G. H. *J. Catal.* **1993**, *143*, 345−368.

(2) Li, P.; Liu, J.; Nag, N.; Crozier, P. A. *Appl. Catal., A* **2006**, *307*, 212−221.

(3) Girardon, J. S.; Quinet, E.; Griboval-Constant, A.; Chernavskii, P. A.; Gengembre, L.; Khodakov, A. *J. Catal.* **2007**, *248*, 143−157.

(4) Rachiero, G. P.; Demirci, U. B.; Miele, P. *Int. J. Hydrogen Energy* **2011**, *36*, 7051−7065.

(5) Bezemer, G. L.; Bitter, J. H.; Kuipers, H. P. C. E.; Oosterbeek, H.; Holewijn, J. E.; Xu, X. D.; Kapteijn, F.; van Dillen, A. J.; de Jong, K. P. *J. Am. Chem. Soc.* **2006**, *128*, 3956−3964.

(6) Den Breejen, J. P.; Radstake, P. B.; Bezemer, G. L.; Bitter, J. H.; Froseth, P. B.; Holmen, A.; de Jong, K. P. *J. Am. Chem. Soc.* **2009**, *131*, 7197−7203.

(7) Bezemer, G. L.; Remans, T. J.; van Bavel, A. P.; Dugulan, A. I. *J. Am. Chem. Soc.* **2010**, *132*, 8540−8541.

(8) Eggenhuisen, T. M.; den Breejen, J. P.; Verdoes, D.; de Jongh, P. E.; de Jong, K. P. *J. Am. Chem. Soc.* **2010**, *132*, 18318−18325.

(9) Shi, L.; Tao, K.; Kawabata, T.; Shimamura, T.; Zhang, X. J.; Tsubaki, N. *ACS Catal.* **2011**, *1*, 1225−1233.

(10) Loveless, B. T.; Buda, C.; Neurock, M.; Iglesia, E. *J. Am. Chem. Soc.* **2013**, *135*, 6107−6121.

(11) Marin, R. P.; Kondrat, S. A.; Gallagher, J. R.; Enache, D. I.; Smith, P.; Boldrin, P.; Davies, T. E.; Bartley, J. K.; Combes, G. B.; Williams, P. B.; Taylor, S. H.; Claridge, J. B.; Rosseinsky, M. J.; Hutchings, G. J. *ACS Catal.* **2013**, *3*, 764−772.

(12) Shi, D. C.; Faria, J.; Pham, T. N.; Resasco, D. E. *ACS Catal.* **2014**, *4*, 1944−1952.

(13) Munnik, P.; Krans, N. A.; de Jongh, P. E.; de Jong, K. P. *ACS Catal.* **2014**, *4*, 3219−3226.

(14) Khodakov, A. Y.; Chu, W.; Fongarland, P. *Chem. Rev.* **2007**, *107*, 1692−1744.

(15) Cronauer, D. C.; Jacobs, G.; Linganiso, L.; Kropf, A. J.; Elam, J. W.; Christensen, S. T.; Marshall, C. L.; Davis, B. H. *Catal. Lett.* **2011**, *141*, 968−976.

(16) Borg, Ø.; Walmsley, J. C.; Dehghan, R.; Tanem, B. S.; Blekkan, E. A.; Eri, S.; Rytter, E.; Holmen, A. *Catal. Lett.* **2008**, *126*, 224−230.

(17) Hong, J.; Chernavskii, P. A.; Khodakov, A. Y.; Chu, W. *Catal. Today* **2009**, *140*, 135−141.

(18) Jacobs, G.; Chaney, J. A.; Patterson, P. M.; Das, T. K.; Davis, B. H. *Appl. Catal., A* **2004**, *264*, 203−212.

(19) Jermwongratanachai, T.; Jacobs, G.; Ma, W.; Shafer, W. D.; Kumaran Gnanamani, M.; Gao, P.; Kitiyanan, B.; Davis, B. H.; Klettlinger, J. L. S.; Yen, C. H.; Cronauer, D. C.; Kropf, A. J.; Marshall, C. L. *Appl. Catal., A* **2013**, *464*−*465*, 165−180.

(20) Shannon, M. D.; Lok, C. M.; Casci, J. L. *J. Catal.* **2007**, *249*, 41−51.

(21) Xiong, H.; Zhang, Y.; Liew, K.; Li, J. *Fuel Process. Technol.* **2009**, *90*, 237−246.

(22) Weststrate, C. J.; Saib, A. M.; Niemantsverdriet, J. W. *Catal. Today* **2013**, *215*, 2−7.

(23) Huang, L.; Xu, Y. *Catal. Lett.* **2000**, *69*, 145−151.

(24) Sun, S.; Fujimoto, K.; Yoneyama, Y.; Tsubaki, N. *Fuel* **2002**, *81*, 1583−1591.

(25) Reinikainen, M.; Niemelä, M. K.; Kakuta, N.; Suhonen, S. *Appl. Catal., A* **1998**, *174*, 61−75.

(26) Bazin, D.; Kovács, I.; Lynch, J.; Guczi, L. *Appl. Catal., A* **2003**, *242*, 179−186.

(27) Cook, K. M.; Poudyal, S.; Miller, J. T.; Bartholomew, C. H.; Hecker, W. C. *Appl. Catal., A* **2012**, *449*, 69−80.

(28) Ragaini, V.; Pirola, C.; Vitali, S.; Bonura, G.; Cannilla, C.; Frusteri, F. *Catal. Lett.* **2012**, *142*, 1452−1460.

(29) Jacobs, G.; Sarkar, A.; Ji, Y.; Luo, M.; Dozier, A.; Davis, B. H. *Ind. Eng. Chem. Res.* **2008**, *47*, 672−680.

(30) Hong, J.; Marceau, E.; Khodakov, A. Y.; Griboval-Constant, A.; La Fontaine, C.; Briois, V. *Chem.—Eur. J.* **2012**, *18*, 2802−2805.

(31) Hong, J.; Marceau, E.; Khodakov, A. Y.; Griboval-Constant, A.; La Fontaine, C.; Villain, F.; Briois, V.; Chernavskii, P. A. *Catal. Today* **2011**, *175*, 528−533.

(32) Morales, F.; Grandjean, D.; de Groot, F. M. F.; Stephan, O.; Weckhuysen, B. M. *Phys. Chem. Chem. Phys.* **2005**, *7*, 568−572.

(33) Rønning, M.; Tsakoumis, N. E.; Voronov, A.; Johnsen, R. E.; Norby, P.; van Beek, W.; Borg, O.; Rytter, E.; Holmen, A. *Catal. Today* **2010**, *155*, 289−295.

(34) Jacobs, G.; Ji, Y.; Davis, B. H.; Cronauer, D.; Kropf, A. J.; Marshall, C. L. *Appl. Catal., A* **2007**, *333*, 177−191.

(35) Jacobs, G.; Ma, W.; Gao, P.; Bhatelia, T.; Bukur, D. B.; Davis, B. H. *Catal. Today* **2013**, *214*, 100−139.

(36) Mohandas, J. C.; Gnanamani, M. K.; Jacobs, G.; Ma, W. P.; Ji, Y. Y.; Khalid, S.; Davis, B. H. *ACS Catal.* **2011**, *1*, 1581−1588.

(37) Jacobs, G.; Ribeiro, M. C.; Ma, W. P.; Ji, Y. Y.; Khalid, S.; Sumodjo, P. T. A.; Davis, B. H. *Appl. Catal., A* **2009**, *361*, 137−151.

(38) Jermwongratanachai, T.; Jacobs, G.; Shafer, W. D.; Rao Pendyala, V. R.; Ma, W.; Kumaran Gnanamani, M.; Hopps, S.; Thomas, G. A.; Kitiyanan, B.; Khalid, S.; Davis, B. H. *Catal. Today* **2014**, *228*, 15−21.

(39) Fonda, E.; Rochet, A.; Ribbens, M.; Barthe, L.; Belin, S.; Briois, V. *J. Synchrotron Radiat.* **2012**, *19*, 417−424.

(40) Payen, E.; Barthe, L.; Berrier, E.; Blanchard, J.; Briois, V.; Carrier, X.; Che, M.; Cristol, S.; Griboval-Constant, A.; Hong, J.; Joly, Y.; Khodakov, A.; La Fontaine, C.; Marceau, E.; Massiani, P.; Tougerti, A. *Act. Chimique* **2011**, *356*−*357*, 20−28.

(41) La Fontaine, C.; Barthe, L.; Rochet, A.; Briois, V. *Catal. Today* **2013**, *205*, 148−158.

(42) Ravel, B.; Newville, M. *J. Synchrotron Radiat.* **2005**, *12*, 537.

(43) Tauler, T. *Chemom. Intell. Lab. Syst.* **1995**, *30*, 133−146.
(44) Carvalho, H. W. P.; Pulcinelli, S. H.; Santilli, C. V.; Leroux, F.; Meneau, F.; Briois, V. *Chem. Mater.* **2013**, *25*, 2855−2867.
(45) Cassinelli, W. H.; Martins, L.; Passos, A. R.; Pulcinelli, S. H.; Santilli, C. V.; Rochet, A.; Briois, V. *Catal. Today* **2014**, *229*, 114.
(46) Voronov, A.; Urakawa, A.; van Beek, W.; Tsakoumis, N. E.; Emerich, H.; Rønning, M. *Anal. Chim. Acta* **2014**, *840*, 20−27.
(47) Jaumot, J.; Gargallo, R.; De Juan, A.; Tauler, R. *Chemom. Intell. Lab. Syst.* **2005**, *76*, 101−110.
(48) Newville, M. *J. Synchrotron Radiat.* **2001**, *8*, 322−324.
(49) Lermontov, A. S.; Girardon, J. S.; Griboval-Constant, A.; Pietrzyk, S.; Khodakov, A. Y. *Catal. Lett.* **2005**, *101*, 117−126.
(50) Yamaguchi, K.; Koike, T.; Kim, J. W.; Ogasawara, Y.; Mizuno, N. *Chem.—Eur. J.* **2008**, *14*, 11480−11487.
(51) Zhan, B. Z.; White, M. A.; Sham, T. K.; Pincock, J. A.; Doucet, R. J.; Rao, K. V. R.; Robertson, K. N.; Cameron, T. S. *J. Am. Chem. Soc.* **2003**, *125*, 2195−2199.
(52) McKeown, D. A.; Hagans, P. L.; Carette, L. P. L.; Russell, A. E.; Swider, K. E.; Rolison, D. R. *J. Phys. Chem. B* **1999**, *103*, 4825−4832.
(53) Rard, J. A. *Chem. Rev.* **1985**, *1*, 1−39.
(54) Osman, J. R.; Crayston, J. A.; Richens, D. T. *Inorg. Chem.* **1998**, *37*, 1665−1668.
(55) Jacob, K. T.; Mishra, S.; Waseda, Y. *J. Am. Ceram. Soc.* **2000**, *83*, 1745−1752.
(56) Okal, J.; Zawadzki, M. *Appl. Catal., A* **2013**, *453*, 349−357.
(57) Lanza, R.; Järås, S.; Canu, P. *Appl. Catal., A* **2007**, *325*, 57−67.
(58) Mousset, F.; Bedioui, F.; Eysseric, C. *Electrochem. Commun.* **2004**, *6*, 351−356.
(59) Mason, R.; Mills, A.; Milton, D. *J. Less-Common Met.* **1989**, *155*, 89−109.
(60) Mun, C.; Ehrhardt, J. J.; Lambert, J.; Madic, C. *Appl. Surf. Sci.* **2007**, *253*, 7613−7621.
(61) Vér, N.; Matus, L.; Kunstár, M.; Osán, J.; Hózer, Z.; Pintér, A. *J. Nucl. Mater.* **2010**, *396*, 208−217.
(62) Song, S. H.; Lee, S. B.; Bae, J. W.; Prasad, P. S. S.; Jun, K. W. *Catal. Commun.* **2008**, *9*, 2282−2286.
(63) Petrovic, S.; Rakic, V.; Jovanovic, D. M.; Baricevic, A. T. *Appl. Catal., B* **2006**, *66*, 249−257.
(64) Mota, N.; Navarro, R. M.; Alvarez-Galván, M. C.; Al-Zahrani, S. M.; Fierro, J. L. G. *J. Power Sources* **2011**, *196*, 9087−9095.
(65) Huffman, G. P.; Shah, N.; Zhao, J.; Huggins, F. E.; Hoost, T. E.; Halvorsen, S.; Goodwin, J. G., Jr. *J. Catal.* **1995**, *151*, 17−25.
(66) Flank, A. M.; Cauchon, G.; Lagarde, P.; Bac, S.; Janousch, M.; Wetter, R.; Dubuisson, J. M.; Idir, M.; Langlois, F.; Moreno, T.; Vantelon, D. *Nucl. Instrum. Methods B* **2006**, *246*, 269−274.
(67) Hu, Z.; von Lips, M.; Golden, M. S.; Fink, J.; Kaindl, G.; de Groot, F. M. F.; Ebbinghaus, S.; Reller, A. *Phys. Rev. B* **2000**, *61*, 5262−5266.
(68) Stavitski, E.; de Groot, F. M. F. *Micron* **2010**, *41*, 687−694.
(69) Sahu, R. K.; Hu, Z.; Rao, M. L.; Manoharan, S. S.; Schmidt, T.; Richter, B.; Knupfer, M.; Golden, M.; Fink, J.; Schneider, C. M. *Phys. Rev. B* **2002**, *66*, 144415.
(70) Lee, Y. S.; Lee, J. S.; Noh, T. W.; Byun, D. Y.; Yoo, K. S.; Yamaura, K.; Takayama-Muromachi, E. *Phys. Rev. B* **2003**, *67*, 113101.
(71) Ko, E.; Kim, B. J.; Kim, C.; Choi, H. J. *Phys. Rev. Lett.* **2007**, *98*, 226401.
(72) Kim, K. J.; Park, Y. R. *Solid. State Commun.* **2003**, *127*, 25−28.
(73) Kogelbauer, A.; Goodwin, J. G., Jr.; Oukaci, R. *J. Catal.* **1996**, *160*, 125−133.
(74) Mhamdi, M.; Marceau, E.; Khaddar-Zine, S.; Ghorbel, A.; Che, M.; Ben Taarit, Y.; Villain, F. *Z. Phys. Chem.* **2005**, *219*, 963−978.
(75) Ben Boubaker, H.; Mhamdi, M.; Marceau, E.; Khaddar-Zine, S.; Ghorbel, A.; Che, M.; Ben Taarit, Y.; Villain, F. *Microporous Mesoporous Mater.* **2006**, *93*, 62−70.
(76) Carrier, X.; Marceau, E.; Che, M. *Pure Appl. Chem.* **2006**, *78*, 1039−1055.
(77) Romero, F. D.; Burr, S. J.; McGrady, J. E.; Gianolio, D.; Cibin, G.; Hayward, M. A. *J. Am. Chem. Soc.* **2013**, *135*, 1838−1844.
(78) Jongsomjit, B.; Panpranot, J.; Goodwin, J. G., Jr. *J. Catal.* **2001**, *204*, 98−109.
(79) Infantes-Molina, A.; Mérida-Robles, J.; Rodrígues-Castellón, E.; Fierro, J. L. G.; Jiménez-López, A. *Appl. Catal., A* **2008**, *341*, 35−42.
(80) Duan, H.; Xu, D.; Li, W.; Xu, H. *Catal. Lett.* **2008**, *124*, 318−323.
(81) Kawano, T.; Takahashi, J.; Okutani, T.; Yamada, T.; Yamane, H. *J. Alloys Compd.* **2009**, *468*, 447−451.
(82) Krstajic, N.; Trasatti, S. *J. Electrochem. Soc.* **1995**, *142*, 2675−2681.
(83) Mota, N.; Alvarez-Galván, M. C.; Navarro, R. M.; Al-Zahrani, S. M.; Goguet, A.; Daly, H.; Zhang, W.; Trunschke, A.; Schlögl, R.; Fierro, J. L. G. *Appl. Catal., B* **2012**, *113−114*, 271−280.
(84) Pirola, C.; Scavini, M.; Galli, F.; Vitali, S.; Comazzi, A.; Manenti, F.; Ghigna, P. *Fuel* **2014**, *132*, 62−70.
(85) Trépanier, M.; Tavasoli, A.; Dalai, A. K.; Abatzoglou, N. *Appl. Catal., A* **2009**, *353*, 193−202.

DOI: 10.1021/cs501799p
ACS Catal. 2015, 5, 1273−1282